NATIONAL ADVISORY COMMITTEE FOR AERONAUTICS

TECHNICAL MEMORANDUM

No. 1122

SYSTEMATIC WIND-TUNNEL MEASUREMENTS ON MISSILES

By O. Walchner

Translation

Systematische Geschossmessungen im Windkanal

Lilienthal-Gesellschaft Report No. 139

Washington

March 1947

NATIONAL ADVISORY COMMITTEE FOR AERONAUTICS

TECHNICAL MEMORANDUM NO. 1122

SYSTEMATIC WIND-TUNNEL MEASUREMENTS ON MISSILES*

By O. Walchner

INTRODUCTION

Wind-tunnel measurements on projectiles are a useful complement to firing tests. In general, the firing tests are limited to the determination of the drag of the shape of the missile. Other problems, such as the determination of the center of pressure and of the air-force components or of the effect of projectile oscillation, and so forth, are not solvable at all by firing tests or only with great difficulties. Such studies are very simple in the wind tunnel.

The Institute for Aerodynamic Research at Göttingen has a small high-speed wind tunnel in which a large number of different nonrotating model projectiles have already been investigated in the range of Mach numbers of 1.2 to 3.2. The tunnel operates on the Prandtl principle, that is, a brief stationary air stream is produced in an evacuated tank by induction of atmospheric air. This mode of operation has become common practice in a number of supersonic tunnels at different research centers and may be regarded as known. The jet dimensions are 110 × 130 millimeters. The size of the models is limited by the condition that the head wave reflected at the jet boundary may not return again to the model itself and must not influence the pressure at the projectile base. Owing to the low density in the air stream it does not succeed, as a rule, to obtain for these dimensions Reynolds numbers high enough to permit figuring with a turbulent boundary layer.

In the first version of the Göttingen tunnel, suction was from the free atmosphere. It was found that the air in the Laval nozzles did not expand adiabatically. It

---

*"Systematische Geschossmessungen im Windkanal," from Lilienthal-Gesellschaft Report No. 139, pp 29-37.

was Wieselsberger who first recognized the condensation of the water vapor contained in the air during the expansion as the cause of this disturbance. It was necessary therefore to calibrate the nozzles for the atmospheric moisture occurring in the course of a year. Figure 1 shows the result of this calibration. The expansion ratio p/p_o is plotted in logarithmic scale against the Mach number (p = pressure in developed jet, p_o = pressure of air at rest). The dashed curve represents the isentropic expansion for air

$$\frac{p}{p_o} = \left(\frac{1}{1 + \frac{\kappa - 1}{2} M^2} \right)^{\frac{\kappa}{\kappa - 1}}$$

with the ratio of the specific heats $\kappa = 1.405$. The expansion of moist atmospheric air yielded the indicated departures from the isentropic curve of seven different Laval nozzles. Since, with increasing moisture content of the inducted air, more heat is continuously released at condensation and this heat input lowers the expansion in a nozzle of specific orifice ratio in increasing measure, the greatest departures from the isentropic curve were observed on sultry summer days, the least on cold winter days. Ludwieg checked this experimentally established result by an approximation. Proceeding from a Laval nozzle of given orifice ratio a combination of momentum continuity and energy equations closely confirmed the described departure from the isentropic curve, when a heat input corresponding to the heat of condensation is introduced in the equation.

Although it thus succeeded in taking into account the effect of the air moisture on the Mach number, the pressure at the nozzle tip and the dynamic pressure, the condensation made itself nevertheless disturbingly noticeable on the quality of the air stream. Naturally the investigation of models in the wind tunnel makes an optimum parallel jet desirable, which in turn requires a well-defined nozzle shape for each Mach number. But, since the Mach number of the same identical nozzle varies with the moisture content of the air, the parallelism of the air stream is for this very reason even only approximately reached, when moist atmospheric air is expanded.

Moreover, in very moist air the water vapor is condensed intermittently (shocklike), where the condensation shock is reflected by the nozzle through the developed jet. At moderate moisture such a shock was avoided by a mild curvature of the nozzles in the area of the condensation region, and the disturbance of the flow by the condensation was already damped out at the nozzle tip.

To improve the testing conditions the tunnel was fitted in 1939 with a silica-gel filter, which extracted the moisture from the air flow. It resulted in a practically perfect adiabatic expansion of air in the Laval nozzles, as indicated in figure 1. The systematic wind-tunnel studies on nonrotating missile models, discussed hereinafter, were all made with dry air.

FORCE DIAGRAM ON THE MISSILE AND ILLUSTRATION ON A WIND-TUNNEL MEASUREMENT (FIG. 2)

A missile exposed at angle of attack α in a flow of speed v is subjected to an air force P with the normal-force component N at right angles to the missile axis and the tangential-force component T along the missile axis. On decomposing the resultant force P in flow direction and at right angle to it, the drag is $W = T \cos \alpha + N \sin \alpha$ and the lift $A = N \cos \alpha - T \sin \alpha$. The distance of the center of pressure from the base is denoted by f and that of the center of gravity by s. The moment of the air force referred to the base is then $M_o = Nf$ and the moment referred to the center of gravity is $M_s = N(f - s)$. The forces and moments are usually expressed by their nondimensional coefficients

$$c_n = \frac{N}{\frac{\rho}{2} v^2 F}, \quad c_t = \frac{T}{\frac{\rho}{2} v^2 F}, \quad c_a = \frac{A}{\frac{\rho}{2} v^2 F},$$

$$c_w = \frac{W}{\frac{\rho}{2} v^2 F} \quad \text{and} \quad c_{m_o} = \frac{M_o}{\frac{\rho}{2} v^2 FD}$$

(ρ = density, F = projectile cross-sectional area, D = caliber or diameter).

By definition the distance of the point of center of pressure from the base is

$$\frac{f}{D} = \frac{c_{m_o}}{c_n}$$

Figure 3 shows an example for the measurement of a model in the tunnel. The projectile has a length of 4 calibers, 2.5 of which are tip and 1.5 cylinder. The ogive merges tangentially in the cylinder. The force and moment coefficients for Mach number 1.99 as well as the position of the center of pressure are plotted against the angle of attack. The tangential force coefficient increases a little with the angle of attack, and the drag coefficient increases even more at greater angles, because a component of the normal force enters in the drag. Lift, normal force, and moment coefficients increase linearly with the angle of attack for small angles. The position of the center of pressure proved to be independent of the angle of attack on this model. The increase of c_t with α and the position of the center of pressure independent of α is not generally applicable but applies specifically to this projectile shape at M = 1.99. Other projectiles show, for example, a c_t independent of α or at greater angles, a relationship between f/D and α. But all the models with the most varied shapes investigated within the framework of the present report exhibited an approximately linear increase of c_n and c_{m_o} with α in the small angle-of-attack range. This result is of practical importance because of its simplicity, as for instance, for the calculation of the spin necessary for stabilization. For, by the gyroscope theory the increase of the moment enters in the condition for a stable flight of spin-stabilized missiles.

RESULTS OF SYSTEMATIC TESTS

Projectiles of identical length with different head shape.- Figure 4 represents six idealized models (without centering collar and rotating bands) of 5 calibers in length each and different head shapes. No. 1 is an ogival-headed missile with an ogival radius of 6.5 calibers and a tip length of 2.5 calibers. On Nos. 5 and 6 the ogival radius is the same as on No. 1, but the tips were shortened by 0.5D and 1.CD, respectively, giving the flattened front areas a diameter of 0.36 and 0.64 calibers, respectively. No. 9 is a cylinder; Nos. 10 and 11 correspond to the shapes 5 and 6, spherical caps with tangential entry being fitted to the flat surfaces and the cylinder lengths shortened by the height of the caps, so that the over-all length amounts to 5 calibers again. The most important test data of this series are represented in figures 5 to 8.

Figure 5 shows the rise in normal-force coefficient with the angle of attack $dc_n/d\alpha$ at $\alpha = 0^\circ$ plotted against the Mach number. With exception of the cylinder, all shapes give a maximum value at around M = 2, while at smaller and greater M somewhat lower values were observed. The comparison of the rise in normal-force coefficient with the angle of attack at fixed Mach number discloses a distinct relationship with the slenderness ratio of the tip. With increasing flattening or rounding, $dc_n/d\alpha$ decreases and assumes the smallest value at the cylinder.

In figure 6 the distance of the center of pressure from the base of the missile $\frac{f}{D} = \frac{dc_{m_o}}{d\alpha} \frac{d\alpha}{dc_n}$ is shown for $\alpha = 0^\circ$ The center of pressure on all shapes travels, with increasing M, toward the base of the missile. This travel is very little on No. 1, but more on the others. The measurements further show for equal Mach number that the air force on the blunt shapes is applied farther forward than on the more slender ones.

With $dc_n/d\alpha$ and f/D for $\alpha \cong 0^\circ$ the increase in the moment M_s, referred to the center of gravity of

the missile, with α is easily computed, which is of importance for the calculation of the stability factor. At a distance s of the center of gravity from the base

$$\frac{dM_s}{d\alpha} = \frac{dc_n}{d\alpha}\left[(f - s)\frac{\rho}{2}v^2F\right]$$

Actually, the term $c_n \frac{df}{d\alpha}\frac{\rho}{2}v^2F$ should be added to the right-hand side of this equation, but it disappears again when interested in the increase of the moment at $\alpha = 0°$, that is, at $c_n = 0$. Besides, f does not vary perceptibly on the shapes involved here at small angles of attack, so that $df/d\alpha = 0$.

Figure 7 shows the drag coefficients for $\alpha = 0°$ plotted against the Mach number. They are of the same order of magnitude at speeds near the velocity of sound for all shapes with exception of the cylinder. With increasing Mach number the drag coefficients of the pointed shape decrease, while those of the blunt heads increase. This behavior is attributable to the different ratio of head drag to suction drag. The coefficient of the suction drag decreases with increasing Mach number and in the extreme case of very high speeds approaches the value zero. For slender missile heads the head drag varies rather little with the Mach number and the total drag coefficient will therefore decrease with the Mach number. On very blunt head shapes, however, the coefficient of the head drag must follow the character of Prandtl's dynamic-pressure formula for supersonic speeds

$$\frac{\Delta p}{\frac{\rho}{2}v^2} = \frac{\kappa + 1}{\kappa}\left[\frac{(\kappa + 1)^2}{4\kappa - 2(\kappa - 1)\frac{1}{M^2}}\right]^{\frac{1}{\kappa-1}} - \frac{2}{\kappa M^2}$$

(Δp = pressure rise in the stagnation point over pressure is undisturbed flow). This formula ensures values which increase with increasing Mach number and at very high speeds approach the limiting value 1.84 for air with $\kappa = 1.405$. But the coefficient of suction drag plays a

subordinate part on very blunt head shapes. According to the measurements, the missiles Nos. 10 and 11 fitted with spherical cap have substantially lower drag coefficients, than the flat-nosed missiles 5 and 6.

Figure 8 represents the effect of the angle of attack on the drag coefficient for shapes 1, 6, and 9 at $\alpha = 0^\circ$ and $\alpha = 6^\circ$. The absolute rise in drag with the angle of attack was found to be about even on the different shapes. But the percentage of increase on the slender missile is much higher than on the blunt shapes. So in order to preserve the beneficial effects of a slender tip on the drag, more care must be given to the pointed than to the blunt missile, so that only small pendulations (angles of attack) occur in flight.

Effect of height of tip for equal over-all length.- A further test series of pointed missiles of the same length of 5 calibers and height of tip of 1.5, 2.5, and 3.5 calibers is shown in figure 9. The data for $dc_n/d\alpha$, f/D, and c_w at $\alpha = 0^\circ$ are represented in figures 10 to 12.

A slight relationship between rise of normal-force coefficient and Mach number with a flat maximum at around $M = 2$ was here also observed (fig. 10). This maximum is less on the long slender tip No. 24 than on the shorter, fuller tip 1 or 22. Compared with figure 5 it is found that $dc_n/d\alpha$ decreases on pointed head shapes with increasing slenderness of tip as well as on blunt shapes with increasing flattening or rounding, and that a short, full tip, say, of shape 22, gives the greatest increases in normal-force coefficient with the angle of attack.

The center of pressure (fig. 11) lies farther forward on the short than on the longer tips, and likewise shows a slight tendency toward the base of the missile at increasing Mach number. But the decrease in f/D becomes consistently less with increasing slenderness of the tip. On shape 24, for example, the applied moment is already practically independent of M and the same holds for the rise in moment coefficient $\frac{dc_{m_o}}{d\alpha} = \frac{dc_n}{d\alpha}\frac{f}{D}$ with α. This

result is also very pleasing, for example, when the curve of precession along the flight path is to be determined.

Again the drag coefficients for $\alpha = 0^\circ$ (fig. 12) exhibit the decrease characteristic of pointed missiles at increasing Mach number. At higher speeds the drag coefficients act approximately inversely proportional to the tip length.

Effect of the cylindrical length for equal head shape.- The deceleration of a missile by the air drag is inversely proportional to the cross-sectional loading (ratio of weight to cross section of missile) and directly proportional to the drag coefficient. A substantial increase in cross-sectional loading to reduce the deceleration of the flying missile for a given caliber is possible only by lengthening the missile. But with increasing length of missile a limit is reached beginning at which the stabilization by rotation becomes difficult. It is therefore particularly important to check the effect of missile length on the air forces and moments in wind-tunnel tests.

Figure 13 shows four missiles of identical tip shape and over-all lengths of 4, 5, 6, and 7 calibers measured at $M = 2.64$. The normal-force coefficients are shown plotted against the missile length for $\alpha = 3^\circ$, 6°, and 9° in figure 14. At small α up to 3° the effect of lengthened cylinder on the normal-force coefficient is very small. Thus in the range of small α the value $dc_n/d\alpha$ is largely dependent upon the shape of the head, and little affected by the cylinder length. At greater α the cylinder contributes a perceptibly increasing portion to the normal force with the length.

The distance of the center of pressure from the missile base at different angles of attack is represented in figure 15. The short missile showed a slight travel of the center of pressure toward the base with increasing angle of attack. With increasing cylinder length this travel is more pronounced because the contribution to the normal force increases at greater angles. For example, on the longest missile of this series the center of pressure

at $\alpha = 10^\circ$ is already by half a caliber farther back than at $\alpha \cong 0^\circ$, and for still longer shapes an even more pronounced travel with the angle of attack is to be expected, as confirmed by several tests (not described here) on several 10-caliber long missiles.

In stability studies, the position of the center of pressure for $\alpha \cong 0^\circ$ is of particular significance. It is reproduced in figure 16 together with the center-of-gravity distance s/D plotted against the missile length l/D. The shift in the position of the center of pressure relative to the tip is very little. Lengthening the missile from 4 to 7 calibers increases the distance of the center of pressure from the tip by about 30 percent. But this distance from the center of gravity is already more than twice as great when homogeneous mass distribution is assumed for the determination of the center of gravity. The moment of the normal force referred to the center of gravity increases, therefore, more than in proportion to the length of the missile as a result of the markedly greater lever arm (f - s).

Lastly, the drag coefficients of this series are plotted against missile length at $\alpha = 0^\circ$, 3°, 6°, and 9° in figure 17. The increase in drag coefficient with the length is small at small α, but greater at greater α, because the component of the normal along the flow increases with the length.

Effect of bow tail on the drag.- Slender missiles are frequently fitted with a bow tail to reduce the air drag. Since low pressure prevails at the base of the missile, the object is to lower the suction drag by reducing the area of the base. However, it should be borne in mind that the air expands more or less around the envelope of the bow tail, depending upon the cone angle, which again acts in the sense of a drag increase.

Figure 18 shows four missiles, the drag coefficients of which are to be compared for axial flow. Shapes 1, 16, and 18 represent a series with constant cone length of $l_k = 0.5D$ and cone angles $\epsilon_k = 0^\circ$, $5^\circ 43'$, and $11^\circ 19'$, while on the series 1, 16, and 21 the cone angle $5^\circ 43'$ is constant and the cone length is 0, 0.5, and 1.0 caliber.

In order to be able to gain some idea of the order of magnitude of the suction drag and an eventual improvement by a bow tail, the ratio of static pressure of undisturbed flow to dynamic pressure

$$\frac{p}{q} = \frac{p}{\frac{\rho v^2}{2}} = \frac{2}{\kappa M^2}$$

is plotted against the Mach number. (See fig. 19.) At complete vacuum on the base of the missile the pressure variation on the base would be equal -p, and on a base area equal to the missile cross section the plotted curve in figure 19 would represent the coefficient of the suction drag, which therefore decreases with rising Mach number and at very high speeds approaches the value zero. Pressure measurements on a number of shapes disclosed, however, only a pressure drop of about one-third of the static pressure of undisturbed flow throughout the entire speed range above velocity of sound. This implies that the coefficient of the suction drag amounts to about one-third of the value p/q only. This amount is rather small at high supersonic speeds and comes into question relative to the total drag only when head and frictional drag together are of similar order of magnitude. Thus at high speeds a decrease in air drag by means of a bow tail can be expected only with particularly slender missile tips, whereas it serves no purpose whatsoever, to fit a blunt missile with it. At speeds near the velocity of sound even a less slender head shape may result in lower drag when the missile is fitted with such a tail.

The drag measurements in the wind tunnel at $\alpha = 0^\circ$ (fig. 20) actually showed at $M = 3$ no perceptible difference in the missiles equipped with this tail compared to the cylindrical form. At decreasing Mach number, however, a noticeable improvement could be observed. The upper part of this figure shows the drag coefficients of the three shapes with equal cone length and different cone angles plotted against the Mach number. The measurements indicate that shape 18 with the greatest cone angle has, in spite of the smaller base

diameter of 0.8D, a greater drag than shape 16 with the least cone and a base diameter of 0.9D. This is attributable to the greater expansion of the air around the bow tail of shape 18. The lower part of figure 20 shows the drag coefficients of the series with equal cone angle and different cone lengths. The drag coefficient decreases monotonic with decreasing base area, although the difference of shapes 16 and 21 is much less than that between 1 and 16.

COMPARISON OF WIND-TUNNEL TESTS AND FIRING TESTS

Because of the limited experience in wind-tunnel measurements at high speeds results of firing tests were used for comparison as far as possible.

In figure 21 the drag coefficients of a bullet measured in the tunnel are compared with firing tests. The agreement is very good. The maximum difference amounts to about $1\frac{1}{2}$ percent.

The agreement was just as close for a blunt missile shape with a drag coefficient $c_w = 0.07$; but less satisfactory for very slender shapes.

Figure 22 shows the recorded drag coefficients of the sS missile at $\alpha = 0^\circ$, 3°, 6°, and 9° plotted against the Mach number. The marked rise in drag coefficient with α on such slender shapes has already been pointed out. The dashed curve represents the average value of the drag coefficients obtained from the time of flight records. The drag coefficients in the firing tests were of the order of magnitude of those measured at $\alpha = 6^\circ$ in the tunnel. However, such a highly developed missile certainly does not oscillate so much in its normal flight that the axis of the missile averages a 6° departure from the tangent to the trajectory. Kutterer (who had made the tests) pointed out, however, that the scattering in his test was fairly great and amounted to about ± 10 percent (shaded area in fig. 22). This scatter is then to be explained by the oscillation of missile rather than by inaccuracies in the time of flight measurement and its interpretation, because the measurements were made directly behind the muzzle. The lower limit of the scatter is therefore the most likely one,

and the difference relative to the wind-tunnel measurements at $\alpha = 0^\circ$ and $\alpha = 3^\circ$ is then no doubt less.

Furthermore, in this comparison, the effect of the Reynolds number on the friction drag must also be allowed for, since it amounts to a perceptible portion of the total drag on such slender missiles. In the wind tunnel the air density at high Mach numbers is very small because the air stream is produced by expansion of the atmospheric air. At $M = 3$, for instance, the Reynolds number referred to the length of a 15 millimeter diameter sS missile model is about 4×10^5, while the natural size sS missile at the same Mach number flies with a Reynolds number of about 2×10^6. Hence a laminar boundary layer and a frictional drag coefficient of around 0.03 referred to missile cross section must be figured with in wind-tunnel tests. The friction layer on the natural size sS missile is turbulent, however, and the coefficient of the friction drag is approximately 0.05. So in the observance of the natural size Reynolds number the total drag measured at $M = 3$ must be raised by about 10 percent, and then the agreement with the firing test will also be substantially better.

Naturally, in the previously discussed wind-tunnel measurements, a corresponding influence of friction drag by the Reynolds number must be taken into account.

The moments measured in the wind tunnel were checked as closely as possible by firing tests. The moments and the position of the center of pressure were measured for a series of systematically lengthened missiles with approximately equal head form. The Rheinmetall Borsig Company, Düsseldorf, fired these missiles with various center-of-gravity positions from barrels with different angles of twist and measured the oscillations of the missiles by firing through pasteboard targets (reference 1). The stability factors

$$\sigma = \frac{I_l^2 \omega^2}{4 I_q \frac{dM_s}{d\alpha}}$$

(I_z = moment of inertia about the longitudinal axis of the missile, I_q = moment of inertia about the transverse axis passing through the center of gravity, ω = angular velocity) were computed with the moment increment $dM_s/d\alpha$ determined in the wind tunnel and compared with the observed oscillation. The stable flight at $\sigma \geq 1.3$ was in close agreement with the gyroscope theory; at smaller stability factors the flight was unstable (oscillations greater than 4°). This result is also a good proof of the correctness of the wind-tunnel measurements. The objection frequently encountered in ballistics that stable flight of missiles required stability factors of the order of magnitude of 10 or 20 was attributable to the lack of a correct conception of the aerodynamic moments involved.

Translated by J. Vanier
National Advisory
Committee for Aeronautics

REFERENCES

1. P. Täubert, Über das Flugverhalten drallstabilisierter Langgeschosse, Forschungsbericht 1534 of the ZWB.

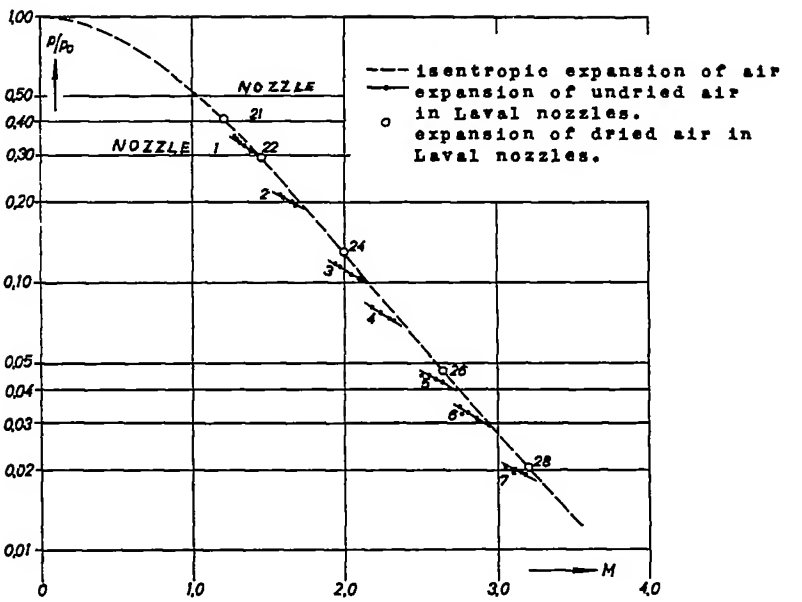

Figure 1. Expansion of dried and undried atmospheric air in Laval nozzles against the isentropic curve.

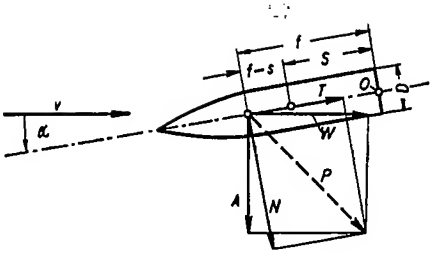

Figure 2. Diagram of forces on a nonrotating missile in oblique flow.

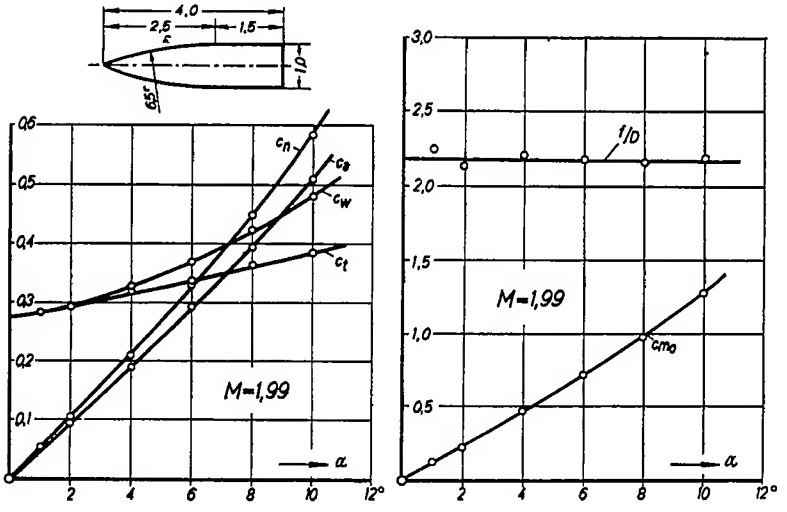

Figure 3. Example of missile test results measured in wind tunnel at M = 1.99.

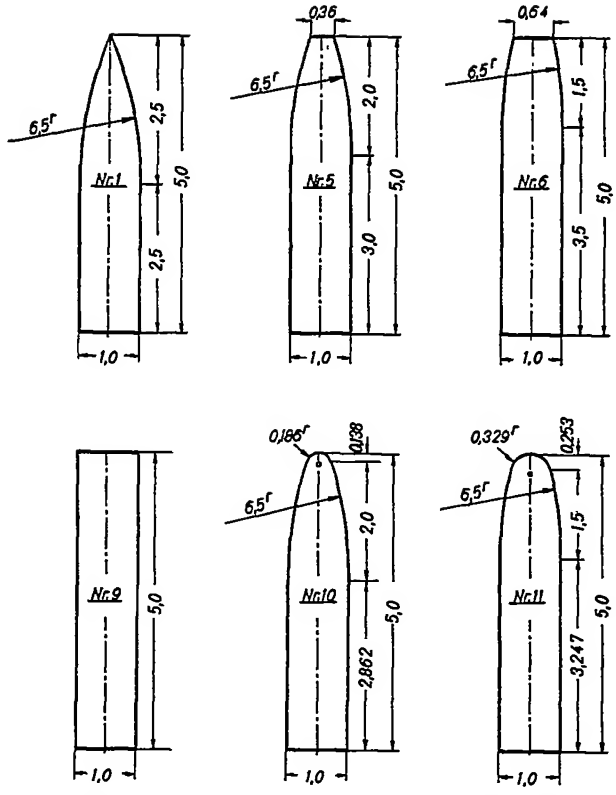

Figure 4. Dimensions of a model series (model Nos. 1, 5, 6, 9, 10, and 11) with different head designs and equal length.

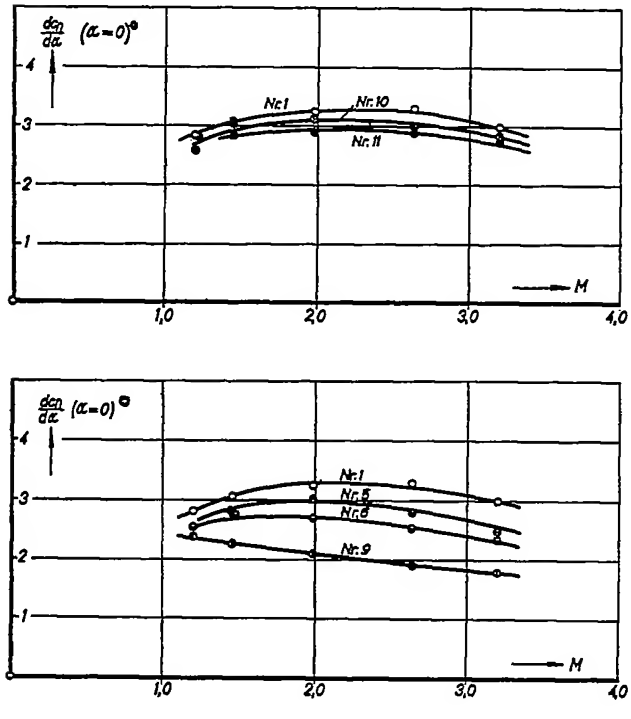

Figure 5. Variation of normal-force coefficient slope with Mach number.

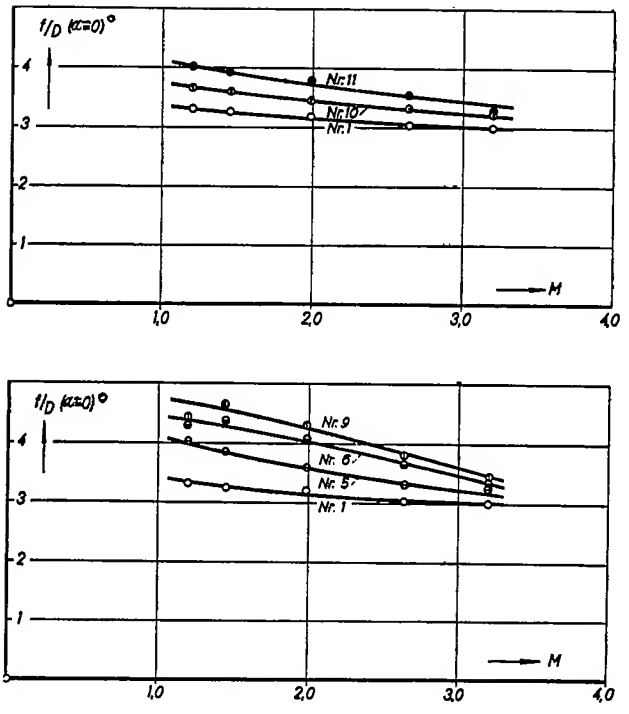

Figure 6. Distance of C. P. from the base of the missile.

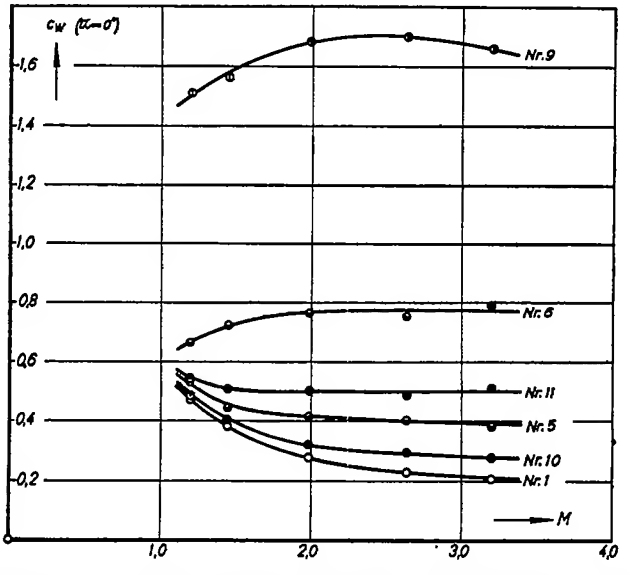

Figure 7. Drag coefficients of models 1,5, 6,9,10, and 11 in axial flow.

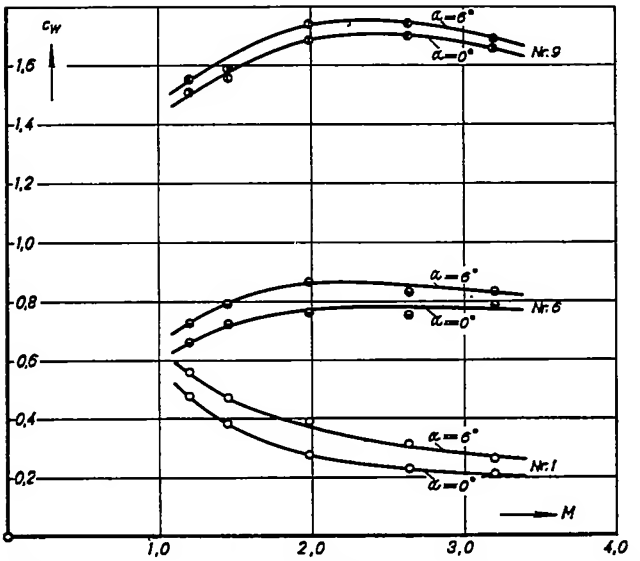

Figure 8. Drag increase due to angle of attack, models Nos. 1,6, and .9.

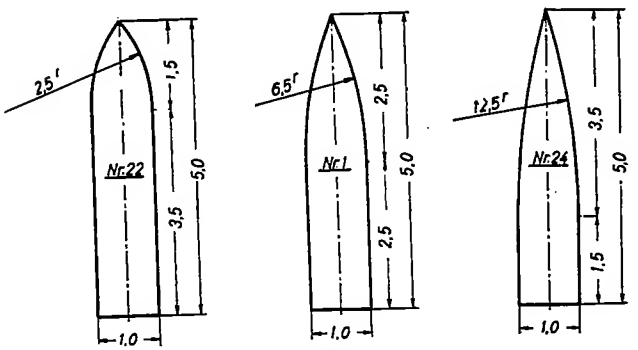

Figure 9. Dimensions of a model series with different tip heights and equal length.

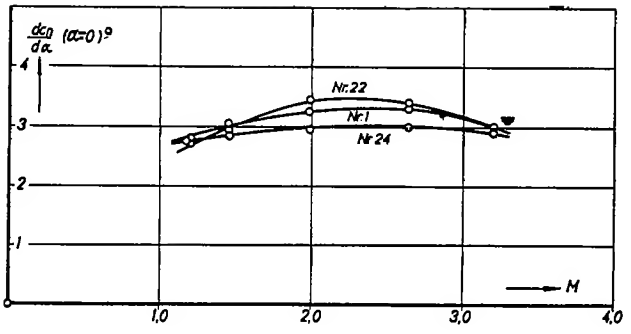

Figure 10. Variation of normal-force coefficient slope with Mach number.

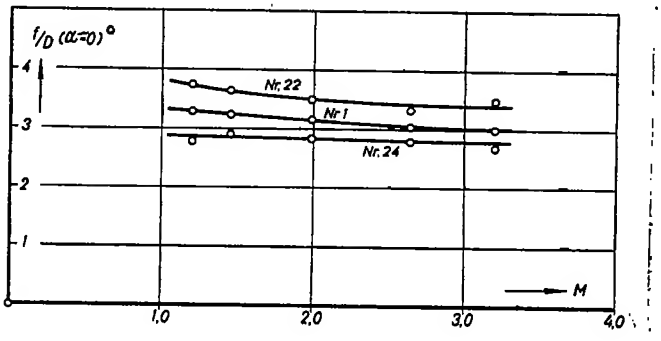

Figure 11. Distance of C. P. from the base.

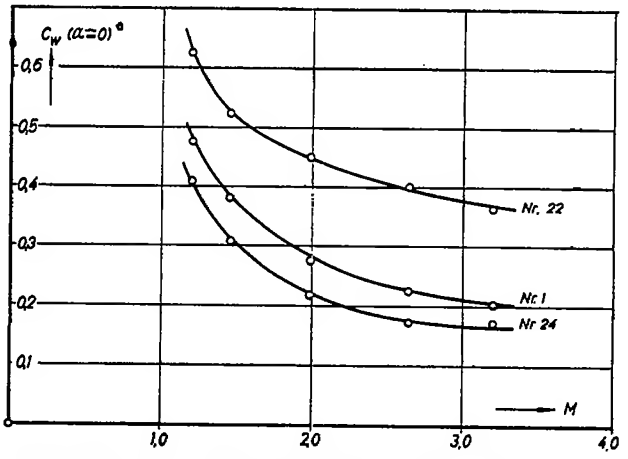

Figure 12. Drag coefficients for axial flow.

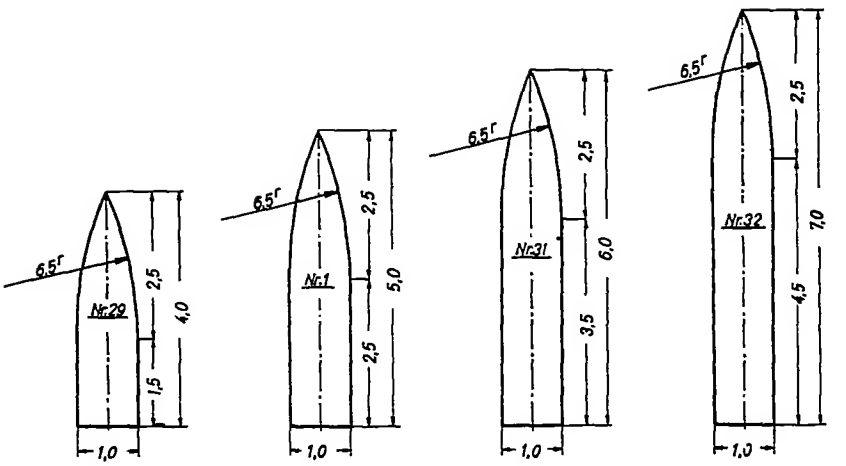

Figure 13. Dimensions of a model series with identical tip and different lengths.

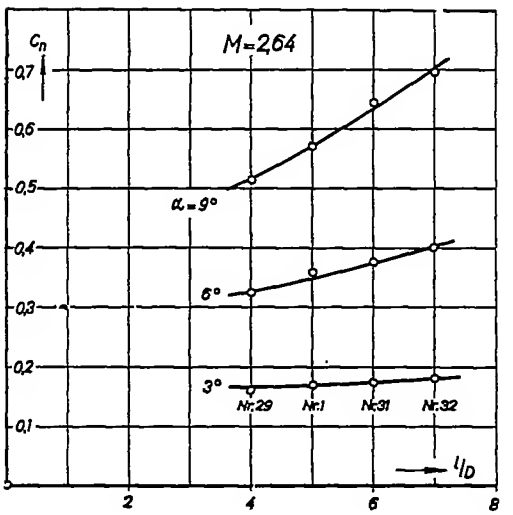

Figure 14. Normal-force coefficient of model Nos. 29, 1, 31, and 32 at M = 2.64 and different angles of attack.

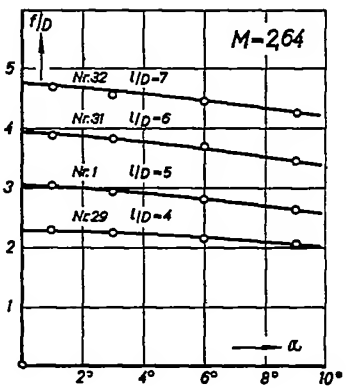

Figure 15. Distance of C. P. from the base with respect to the angle of attack.

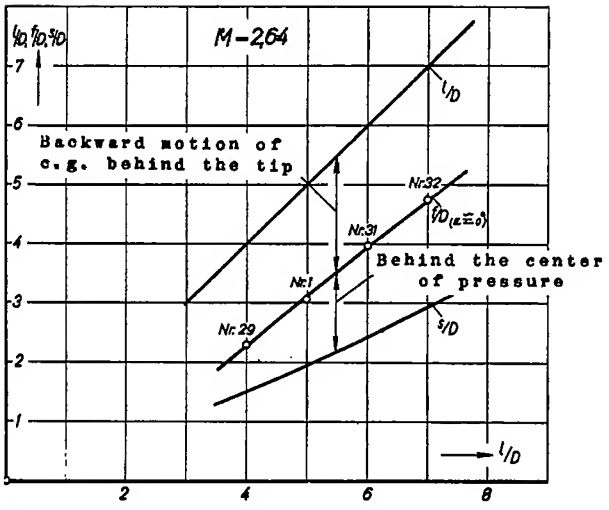

Figure 16. Position of C.P. at small angles of attack $\alpha \cong 0°$ and M= 2.64 relative to tip and center of gravity.

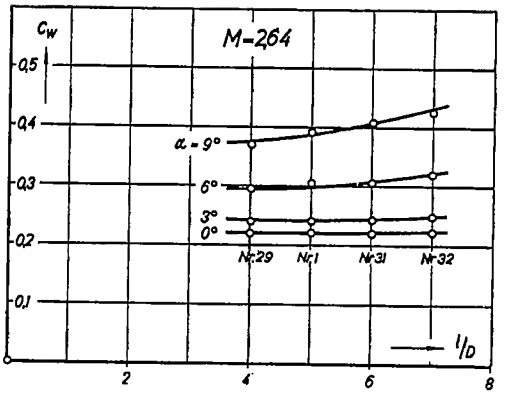

Figure 17. Drag coefficients of models Nos. 29, 1, and 32 at M= 2.64 and various angles of attack.

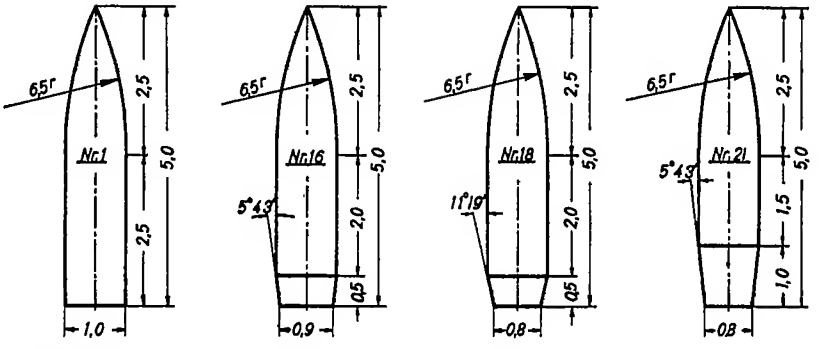

Figure 18. Dimensions of model series with different bow tails for equal tip shape and over-all length.

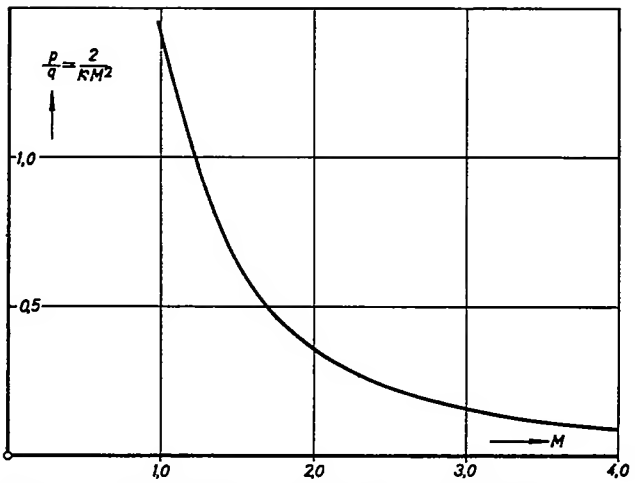

Figure 19. Ratio of static pressure p in undisturbed flow to dynamic pressure $q=\frac{p}{2}v^2$ plotted against Mach number.

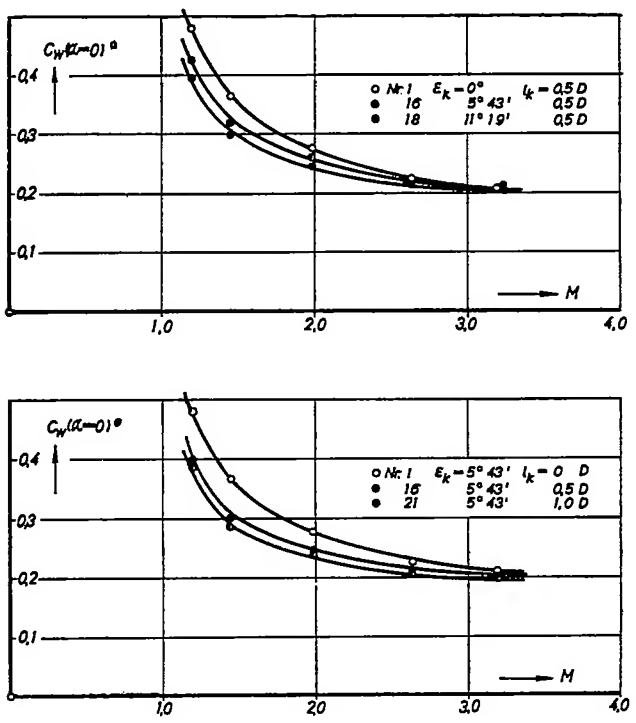

Figure 20. Drag coefficients for axial flow, Models 1, 16, and 18 with equal cone length and different cone angles (top). Models 1, 10, and 21 with equal cone angles.

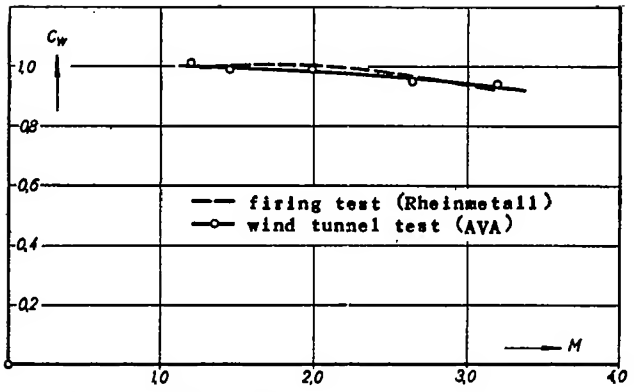

Figure 21. Drag coefficient of bullets-comparison of firing test and wind-tunnel test.

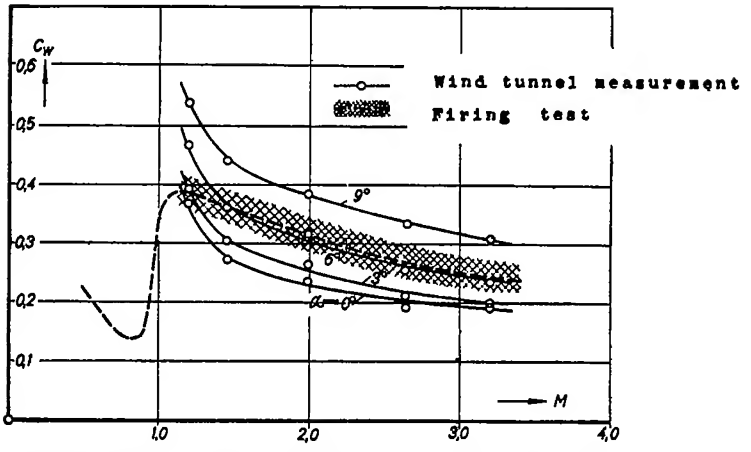

Figure 22. Drag coefficient of the sS missile-comparison of firing test with wind-tunnel test.